Research article

Synthesis of high surface area mesoporous ZnCl$_2$–activated cocoa (*Theobroma cacao* L) leaves biochar derived *via* pyrolysis for crystal violet dye removal

Jamiu Mosebolatan Jabar [a,*], Matthew Ayorinde Adebayo [b], Ignatius Adekunle Owokotomo [a], Yisau Adelaja Odusote [c], Murat Yılmaz [d]

[a] *Textile and Polymer Research Laboratory, Chemistry Department, The Federal University of Technology, P.M.B. 704, Akure, Nigeria*
[b] *Physical Chemistry Laboratory, Chemistry Department, The Federal University of Technology, P.M.B. 704, Akure, Nigeria*
[c] *Condensed Matter and Statistical Physics, Department of Physics, The Federal University of Technology, P.M.B. 704, Akure, Nigeria*
[d] *Department of Chemical Engineering, Faculty of Engineering, Osmaniye Korkut Ata University, 80000, Osmaniye, Turkey*

ABSTRACT

Chemically activated cocoa leaves biochar (CLB) was successfully prepared from fallen cocoa leaves (CLs) *via* ZnCl$_2$–activation and pyrolysis at 700 °C for sequestration of toxic crystal violet (CV) dye from aqueous solution. CLs and CLB were characterized using elemental analysis (CHN/O), Brunauer-Emmett-Teller method (BET), thermogravimetric analysis (TGA), Fourier transform infrared (FTIR), X-ray diffraction (XRD) spectroscopy and scanning electron microscopy (SEM). The optimum conditions for effective removal of CV dye from aqueous solution (75.67% for CLs and 99.87% for CLB) were pH 9, initial CV dye concentration 100 mg/L, adsorbent (CLs/CLB) dose 0.4 g/L, contact time 160 min and temperature 300 K. Modified Ritchie second order best described kinetic and Liu model described equilibrium adsorption. CLs and CLB with maximum adsorption capacities 190.70 and 253.3 mg/g respectively, compete favorably with adsorbents used for removal of CV dye from wastewater in the literature. The high BET surface area (957.02 m^2/g) and mean pore diameter (7.21 nm) were indicators of better adsorption efficiency of CLB. CLs showed adsorption to proceed towards endothermic process, while it was exothermic process for CLB. This study established the suitability of cocoa leaves as sustainable and environmental friendly precursor for preparation of adsorbent for the treatment of dye-containing wastewater.

1. Introduction

Concerns about water scarcity seen in different parts of the world are constantly increasing as a result of the continuous pollution of existing waters by various factors. Among these factors are chemical compounds like dyes [1], pesticides [2], heavy metals [3], drugs and emerging contaminants [4] which are the leading factors that pollute the ecosystem. These substances are released into the environment *via* industrial, hospital or domestic wastewater [5]. Among these pollutants, dyes are eye-saw in wastewater owing to their color. Often used dyes in textile, leather, plastic, cosmetics etc are synthetic ones [6]. The ecological balance and human health are negatively affected by these synthetic dyes due to their non-biodegradable, toxic and carcinogenic properties [7]. About 10–20% of the dyestuffs entering the process are discharged into water bodies as unprocessed dyestuffs, which is

estimated to be an average of (0.7–2.0) $\times 10^5$ tons per year [8]. These synthetic dyes can be divided into three main classes: azo, triphenylmethane and anthraquinone dyes. Triphenylmethane dyes are of high interest among synthetic dyes because of their toxicity [9]. The main ones are crystal violet, brilliant green, victoria blue B, malachite green, basic fuchsine, methyl green and aniline blue. These dyes find application in various sectors from textile to paper printing, from tropical medicine to the furniture industry etc. Research studies revealed that these dyes cause damage to the heart, kidney, spleen, liver, eyes, lungs, skin, bones and have teratogenic effects in the brain and nervous system [7].

Crystal violet (CV) from the triaphenylmethane family is a synthetic cationic dye also known as aniline violet, gentian violet, or pyocyanin. It is frequently found in industrial wastes due to its extensive applications in medicine as a biological stain, colorant, anthelmintic, bacteriostatic

---

and antimicrobial agent in the detergent, textile, fertilizer and printing industry. CV is a dye with cytotoxic and mutagenic effects, it can also damage the cornea (leading to permanent blindness), the gastrointestinal, and respiratory systems if consumed [10].

Thus, CV dye removal is mandatory before discharging CV-contaminated wastewater into water body to circumvent possible health hazard associated with it. There are many methods to treat dye-house effluent and the main ones can be classified as chemical oxidation [11], ozonation [12], electrochemical [13], coagulation/-flocculation [14], membrane filtration [15], photo-degradation [16], biological [17], precipitation [18] and adsorption process [19, 20, 21]. Among these methods, adsorption is preferred because of its simplicity and high removal efficiency. However, researchers are trying to synthesize more efficient and cheaper adsorbent materials (biochars) as alternative to commercial activated carbons (often used in the adsorption process) with high processing and production costs [7].

The trend towards biochar, which has been shown as a viable alternative adsorbent, is increasing day by day because it is sustainable, environmentally friendly and cheap [5]. Biochar, which is obtained from biomass as raw materials, also prevents agro-byproducts from being wasted [22, 23]. In addition, the amount of carbon dioxide released into the atmosphere will reduce with the widespread use of biochar [22]. Enhancing the functional groups, surface area and pore volume by modifying the surface of biochar would be an effective method for removing dyes from wastewater. The methods used to modify/activate biochar surfaces are physical and chemical activation processes. Chemical activation has been reported to be more effective than physical activation in the literature [22]. In physical activation, the raw material is carbonized at high temperature under an inert atmosphere, carbon dioxide (CO_2) or water vapor. While in chemical activation, the raw material is carbonized by reacting it with chemicals such as $ZnCl_2$, KOH, NaOH, Na_2CO_3, H_2SO_4, HNO_3 and H_3PO_4 in an inert environment at high temperature. $ZnCl_2$ as chemical activating agent is gaining more popularity due to its ability to facilitate production of biochar with high mesoporous surface area. Zn^{2+} occupies wide space in carbonaceous matrix when $ZnCl_2$-impregnated biomass is carbonized. Washing (with water) of the chemically activated biochar leaches out Zn^{2+} to insert pores of high surface area and volume onto the synthesized activated biochar. The high porosity boosts the diffusion and adsorption of the large molecular weight dye and other emerging contaminants from wastewater onto the pores of the $ZnCl_2$-activated biochar [23]. The leachate generated from the synthetic process of a $ZnCl_2$-activated biochar must be properly disposed to circumvent heavy metal-environmental pollution. There are many studies in the literature on the use of activated carbons obtained from agricultural biomass in the removal of pollutants. Oil palm empty fruit bunch fiber [1], almond leaf [5], water lily stem [7], Chinar leaf [8], corncob [24], elephant grass [25] and cocoa pod [26] are some of these biomasses.

Cocoa (*Theobroma cacao* L) is an important crop for countries such as Africa, countries in the tropics and subtropics of Southeast Asia and Latin America as the world's largest producers [27]. It flowers and fruits between 3 and 5 years of plantation, the seeds from mature fruits are major ingredient used in the manufacture of various foods such as beverages, chocolate, ice-cream, baked goods etc. It is one of the main products exported by some developing countries like Nigeria to earn foreign currency [22]. Cocoa cultivations are encouraged in these countries because of the low initial capital investment and well-established traditional plant protection approach [28]. During the dry season, cocoa tree sheds off many of its leaves to conserve available water through reduction the in rate of transpiration [5]. The fallen leaves cause environmental mess and conversion of these fallen leaves to adsorbent will serve dual purposes, ranging from production of wealth from waste to environmental tidiness. In the literature, limited studies have been carried out on the use of fallen CLs and their derivatives as adsorbents for removal of pollutants such as dyes, emerging contaminants and heavy metals from wastewater. Other

reasons why CLs were chosen for this study are their abundance, sustainability and non-existing competitive use in Nigeria. Overall, $ZnCl_2$-activated cocoa leaves biochar has not been reported for removal of dye from dye contaminated wastewater in the literature.

In this study, cocoa leaves biochar (CLB) was prepared from the cocoa leaves (CLs) through $ZnCl_2$ activation and was its efficiency in removing CV dye from an aqueous solution was evaluated. Parameters such as the pH of the solution, the initial concentration of the adsorbate, the contact time between the adsorbent and the adsorbate, the influence of the adsorbent dose and adsorption temperature were examined as the removal conditions for CV dye from aqueous solution. Thermodynamics, kinetics and isotherms for CV dye adsorption onto CLs and CLB adsorbents were studied to design an efficient treatment plant for wastewater polluted by CV dye and other related large molecular weight organic compounds.

2. Materials and methods

2.1. Materials

Cocoa leaves (CLs) were obtained from a cocoa farm at Itaoniyan rural settlement, along old Akure/Ondo road, Akure, Ondo State, Nigeria. The plant leaves were authenticated by the Forestry and Wood Technology Department, the Federal University of Technology, Akure. CV dye stuff (Fig. S1), $ZnCl_2$, HCl, NaOH and other chemical reagents used were acquired from Sigma-Aldrich Chemie, Germany.

2.2. Preparation and characterization of CLs and CLB

CLs were thoroughly washed using distilled water to clean them off the dust, sand other related fouls. CLs (100 g) was then oven-dried at 110 °C for 3 h, weighed and returned to the oven for further drying at 110 °C for 10 min and reweighed. Drying (at 110 °C for 10 min) and weighing were continued until a constant weight was obtained. The dried CLs were ground to particle size between 150 and 200 μm. CLs (20 g) were retained for further processing. $ZnCl_2$ activated cocoa leaves biochar (CLB) was prepared as described by Thue et al. [23] with little modification. About 77 g (the remaining part) of CLs were impregnated with $ZnCl_2$ (30 %wt) at liquor ratio 1:1.5 in a beaker (1000 mL) and heated to temperature between 70 and 75 °C for 4 h with continual stirring on the heating mantle. The $ZnCl_2$-impregnated CLs were left open at room temperature to age for the next 20 h. The $ZnCl_2$-impregnated CLs were subjected to pyrolysis in a pyrolyzer by raising the temperature of the reactor to 700 °C within 1 h at a heating rate of 10 °C min^{-1} under nitrogen atmosphere at a flow rate of 150 mL/min. The pyrolyzer was cooled to 30 °C at a rate of 50 °C min^{-1} and CLB was obtained. CLB was washed with 0.5 M HCl, followed by thorough washing with distilled water to bring the pH of the biochar to 7 and dried in an oven at 110 °C for 3 h. Drying (110 °C for 10 min) and weighing were continued for 10 min consecutively until a constant weight was obtained. The leachate from the CLB washing was properly disposed through the waste chemical disposing agent to circumvent heavy metal-environmental pollution. The prepared biochar (CLB) and dried leaves (CLs) were ground to particle size between 80 and 100 μm, kept for characterization and adsorption process.

2.3. Characterization of CLs and CLB

Moisture content (MC) of CLs and CLB was determined from weight of the adsorbent before (w_1) and after oven drying (w_2) (Eq. 1), while CLB yield (Y) was evaluated from weight of oven dried biochar (w_3) and weight of oven dried CLs (w_2) (Eq. 2).

$$MC\ (\%) = \frac{w_1 - w_2}{w_1} x 100\% \qquad (1)$$

$$Y\ (\%) = \frac{w_2 - w_3}{w_2} x 100\% \tag{2}$$

Buck densities (BD) (g/mL) of CLs and CLB were determined using Eq. (3), by weighing empty density flask (5 mL) (w_4) and sample filled density flask (w_5). v_1 is the volume of density flask.

$$BD = \frac{w_5 - w_4}{v_1} \tag{3}$$

Determination of ash content (AC) was done by placing crucible containing pre-weighed adsorbent (CLs and CLB) in the furnace for 5 h at 650 °C. Drying and weighing were continued for 10 min consecutively until a constant weight was obtained. AC was evaluated using Eq. (4).

$$AC = \frac{w_6 - w_7}{w_8 - w_7} x 100\% \tag{4}$$

Where weight of crucible containing ash is w_6, w_7 is the weight of empty crucible and w_8 is the weight of crucible containing dried adsorbent (CLs or CLB).

CLs and CLB were characterized by elemental analysis (CHN/O), Brunauer-Emmett-Teller method (BET), thermogravimetric analysis (TGA), Fourier transform infrared spectroscopy (FTIR), scanning electron microscopy (SEM) and X-ray diffraction analysis (XRD).

2.4. Preparation crystal violet solution

CV dye stock solution (100 mg/L) was prepared as reported elsewhere [2]. Standardization of CV dye solution was done through scanning of dye aliquot in UV–Vis spectrophotometer (Pharmacia LKB Biochrome 4060). Calibration curves were plotted (concentration varied from 20 to 100 mg/L) for each of the pH values (1–11) at each of the corresponding wave lengths of maximum absorption (λ_{max}) to account for variation in CV color as pH value altered from 1–11. The adsorbed CV dye concentration interpolated from each of the calibration curves was used to determine the percentage CV dye removed and adsorption capacities of CLs and CLB at each of the pH values. The pH value with the highest percentage CV dye removal was chosen for the batch adsorption process [7].

2.5. Adsorption experiments

The optimum CV dye adsorption from dye solution (100 mL) was assessed through batch the adsorption process. Adsorption parameters such as pH, initial dye concentration, adsorption dose, time, and temperature were varied to establish optimum conditions for dye-uptake (Eq. 5) and percentage CV dye adsorbed (Eq. 6) from dye solution. At the end of the adsorption process, each of the treated solutions was centrifuged at 4500 rpm for 10 min. An aliquot of each of the centrifuged treated samples was obtained with a syringe (1 mL) and analyzed via UV-Vis spectrophotometer for calculating dye-uptake and percentage CV dye adsorbed [1].

$$q_e = \left(\frac{c_x - c_y}{w}\right) v \tag{5}$$

$$R(\%) = \left(\frac{c_x - c_y}{c_x}\right) 100\% \tag{6}$$

Where q_e (mg/g) is the dye-uptake, c_x and c_y (mg/L) are the dye concentrations before and after adsorption process, respectively, v (L) is the volume of CV dye solution and w (g) is the weight of CLs and CLB.

2.6. Modeling of kinetic and equilibrium data

For elucidation and interpretation of the kinetic data, the data obtained from the effect of contact time were subjected to five nonlinear kinetic models. These models are pseudo-first order, pseudo-second order, modified Ritchie second order, Avrami fractional order, and intraparticle diffusion models [1, 7, 24, 29]. The mathematical representations of these models are summarized in Table 1.

Three nonlinear equilibrium models employed for the interpretation of equilibrium data are Freundlich, Langmuir, and Liu [7, 30]. The mathematical representations of these models are summarized in Table 2.

2.7. Statistical evaluation

Two statistical expressions {adjusted correlation coefficient (R^2_{adj}) and standard deviation (SD)} were used to adjudge the fittingness of the kinetic and equilibrium data to the nonlinear models. Eqs. (7) and (8) present the respective statistical expressions of R^2_{adj} and SD.

$$R^2_{adj} = \left\{1 - \left(1 - R^2\right)\right\} \left\{\frac{n-1}{n-p-1}\right\} \tag{7}$$

$$SD = \sqrt{\left\{\frac{1}{n-p}\right\} \sum_i^n \left(q_{i,\exp} - q_{i,\text{model}}\right)^2} \tag{8}$$

where R^2 = determination coefficient, n = the number of experiments carried out, p = number of parameters present in a model, q = numerical value of the data, and $q_{i,model}$ and $q_{i,exp}$ = predicted q value by a model and experimentally measured q value, respectively. Standard deviation

Table 1. Mathematical equations for kinetic models.

Models	Mathematical expression	Parameters	References
Pseudo-first order	$Q_t = Q_e\{1 - \exp(-k_f t)\}$	Q_t and Q_e = amounts (mg) of CV dye adsorbed by 1 g of CLs or CLB at time, t and equilibrium, respectively; k_f = pseudo-first order rate constant (1/min).	[7]
Pseudo-second order	$Q_t = Q_e - \frac{Q_e}{k_s Q_e t + 1}$	k_s = pseudo-second order rate constant (g/mg min)	[7]
Modified Ritchie second order	$Q_t = Q_e\left\{1 - \frac{1}{k_{mR}t + \beta}\right\}$	k_{mR} = modified Ritchie second order rate constant (1/min); β = Ritchie's constant (this is related to initial loading of the pollutant on adsorbent) (1/min).	[29]
Avrami fractional order	$Q_t = Q_e\{1 - \exp(-k_{Av}t)^{n_{Av}}\}$	k_{Av} = Avrami fractional order rate constant (1/min); n_{AV} = Avrami's fractional order (this is related to mechanism of adsorption).	[24]
Intraparticle diffusion	$Q_t = k_{ipd}\sqrt{t} + C$	k_{ipd} = intraparticle diffusion rate constant (mg/g min$^{0.5}$); C = intraparticle diffusion constant (this is related to the thickness of the boundary layer (mg/g)	[1]

Table 2. Mathematical equations for equilibrium models.

Models	Mathematical expression	Parameters	References
Freundlich	$Q_e = K_F C_e^{\frac{1}{n_F}}$	C_e = equilibrium concentration of CV (mg/L); K_F = Freundlich equilibrium constant $(mg/g)(mg/L)^{-\frac{1}{n_F}}$; n_F = Freundlich's exponent	[7]
Langmuir	$Q_e = \frac{Q_{max} K_L C_e}{1 + K_L C_e}$	Q_{max} = maximum adsorption capacity of the adsorbent (mg/g); K_L = Langmuir equilibrium constant (L/mg)	[7]
Liu	$Q_e = \frac{Q_{max}(K_g C_e)^{n_g}}{1 + (K_g C_e)^{n_g}}$	K_g = Liu equilibrium constant (L/mg); n_g = dimensionless Liu's exponent.	[30]

Table 3. Characteristics of CLs and CLB.

Properties	Unit	Magnitude	
		CLs	CLB
Yield (Y)	wt %	-	41.17
Moisture content (MC)	wt %	2.90	1.98
Bulk density (BD)	g/mL	0.83	0.46
Ash content (AC)	wt %	7.37	13.59
Carbon (C)	wt %	42.59	57.83
Hydrogen (H)	wt %	6.42	3.92
Nitrogen (N)	wt %	1.69	0.58
Oxygen (O by difference)	wt %	49.30	37.67
Total pore volume (cm^3/g)	cm^3/g	0.49	1.35
Micropore volume (cm^3/g)	cm^3/g	0.41	0.13
Mesopore volume (cm^3/g)	cm^3/g	0.08	1.22
Mean pore diameter (nm)	nm	1.87	7.21
Surface area (S_{BET})	m^2/g	365.57	957.02

values determine the numerical difference between the values of $q_{i,model}$ and $q_{i,exp}$. The smaller the value of SD, the smaller the difference between $q_{i,model}$ and $q_{i,exp}$, hence, the better the fit of the data to a fitting model [31, 32]. In another dimension, the closer the value of R^2_{adj} to unity, the better the fitness of the data to the model [33].

3. Results and discussion

3.1. Characterization of CLs and CLB

Table 3 shows physicochemical, textural properties and elemental analysis of CLs and CLB. CLB has a relatively high yield when compared with the ones reported by some researchers in the literature for biomass-derived biochar through pyrolysis for wastewater treatment [34, 35]. This indicated the feasibility of scaling up the production of this adsorbent for industrial application in treatment of industrial effluents. Low moisture content and bulk density displayed porous (hollow) structure of CLB according to Jawad et al. [36]. The high ash content of CLB might be resulted from absorption of part of the metallic zinc during chemical activation of CLs.

The CLs and CLB elemental analysis was carried out using Perkin Elmer CHN analyzer at 1800 °C and oxygen content was determined at 1400 °C under nitrogen environment [7]. The higher carbon, lower nitrogen, hydrogen and oxygen contents of CLB when compared with those of CLs might be due to dehydration and carbonization of CLs during $ZnCl_2$ activation and pyrolysis process [5].

N_2 sorption curves and pore size distributions of CLs and CLB at 77 K are presented in Figure 1a and b respectively. The N_2 sorption curve of CLs showed type II sorption isotherm, while that of CLB displayed hysteresis loop that could be associated with type IV isotherm based on the International Union of Pure and Applied Chemistry (IUPAC) classification. CLB adsorption-desorption curves as Type IV isotherm are similar to those of mesoprous activated biochars reported for treatment of wastewater in the literature [7, 23]. The Type IV isotherm indicated multilayer coverage at low pressure after monolayer formation [34]. The average pore diameter of CLB >20 Å confirmed that its structure to be more of mesoporous than microporous. This CLB attribute was quite opposite for CLs with pore diameter <20 Å according to IUPAC definition (Table 3). Transformation of CLs diameter from microporous to mesoporous structure after its conversion to CLB could be traced to pyrolysis, chemical activation and leaching-out of metallic zinc from the activated biochar [23]. The high BET surface area of CLB affirmed its acceptability as a potential sustainable adsorbent for treatment of wastewater.

The thermal stability of CLs and CLB were assessed using a thermogravimetric analyzer (Shimadzu TG 50, Japan) operated from 28 to 600 °C under nitrogen gas and 600–900 °C under oxygen gas at a heating rate of 10 °C/min [5]. TGA thermograms for CLs and CLB show incipient and other two degradation stages (Figure 1c). The incipient degradation stage from 28 to 171.29 and 28–182.92 °C might be linked to evaporation of moisture in CLs and CLB with weight loss of 2.90 and 1.98% respectively [7]. The second weight loss (18.30%) between 171.29 and 388.20 °C for CLs might be due to the decomposition of pectin, hemicellulose and part of cellulose. In CLB, the second weight loss (13.93%) that occurred between 182.92 and 393.23 °C might be due to evaporation of volatile organic compounds and decomposition of part of carbonaceous materials [5]. The final decomposition stage in CLs could be associated with the degradation of lignin and the remaining part of cellulose at temperature between 388.20 and 579.67 °C with weight loss of 53.47%. Equally, the final degradation stage that could be traced to the decomposition of carbon skeleton in CLB occurred between 393.20 and 587.72 °C with 46.90% corresponding weight loss [5]. These observations showed that CLB is more thermally stable than CLs.

FTIR spectrophotometer (Perkin Elmer) operated at 4 cm⁻¹ resolution with 64 scans and wavenumber between 400 and 4000 cm⁻¹ (Figure 1d) was used for assessing functional groups present at the surfaces of CLs and CLB. The broad spectral at 3352 and 3372 cm⁻¹ could be traced to the presence of OH and/or N–H functional groups in CLs and CLB respectively according to the previous study [6]. The peaks at 2976 and 2857 cm⁻¹ could be attributed to C–H asymmetric and symmetric stretching vibration in CLs and CLB respectively [1]. The characteristic peaks at 1743 and 1719 cm⁻¹ could be assigned to C=O in CLs and CLB respectively [25], peak reduction noticed after pyrolysis (CLB) might be due to evaporation of volatile matters. The characteristic bands at 1241 and 1252 cm⁻¹ affirmed the presence of C–O functional group of organic moieties in CLs and CLB respectively. The vibration peaks at 1011 and 1001 cm⁻¹ confirmed the presence of –OH functional group of moisture in both CLs and CLB According to Jabar et al. [5].

SEM results of CLs and CLB are presented in Figure 1e and f. CLs have irregular-shaped rough surface morphology with quite a lot of micropores. These qualities established CLs as a potential adsorbent for the removal of pollutants from wastewater according to [37]. CLB displayed a well-developed high surface area with mesoporous structure dominating microporous structure (Figure 1 d). These observations upheld our findings in the N_2 sorption analysis of CLs and CLB.

Fig. S2 displays XRD crystallographic diffraction patterns of CLs and CLB. The XRD pattern of CLs demonstrates major broad shoulders at $2\Theta = 28.9°$ and $53.8°$ that correspond to (102) and (105) respectively of the lignocellulosic biomass' amorphous nature according to standard
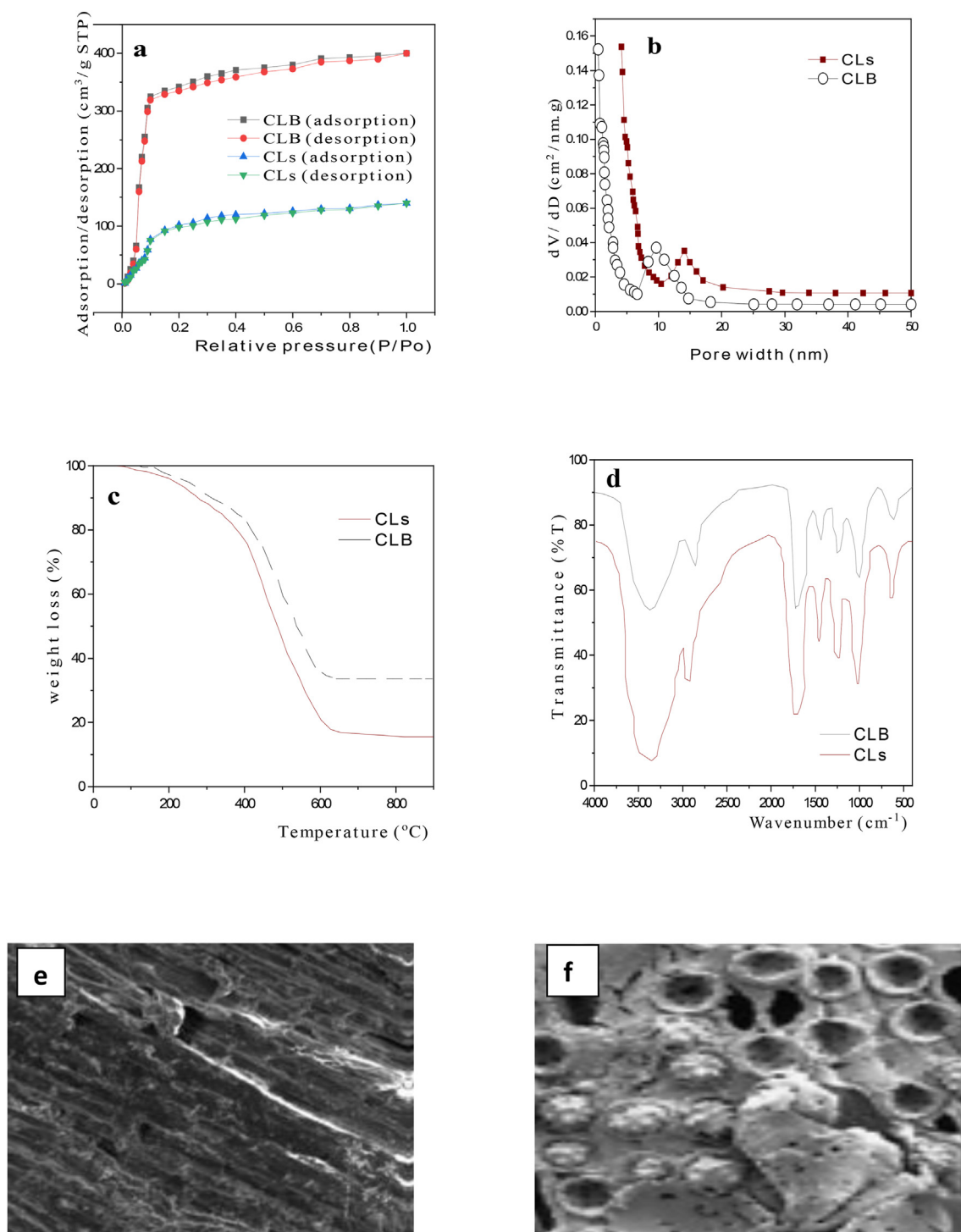
Figure 1. BET surface area (a), mean pore diameter (b), thermogravimetric analysis (c), FTIR spectra (d), morphologic structures of CLs (e) and CLB (f).

diffraction reference pattern (PC PDF No: 898487). The evolved new broad peaks at $2\Theta = 23.1°$ (002) and $40.4°$ (101) besides the moderate broad shoulder at $2\Theta = 54.2°$ (105) by CLB affirmed conversion of CLs to amorphous carbon after pyrolysis according to Jabar et al. [1].

3.2. Adsorption studies

3.2.1. Effect of pH

The adsorption process is strongly influenced by the pH of the solution, because it determines the affinity of aqueous dye solution for hydroxyl, carboxyl and amino functional groups on the adsorbent surface

[7]. The mechanism of adsorption of CV dye onto CLs and CLB was investigated by the varying pH of the dye solution from 1 – 11 at fixed initial CV dye concentration (100 mg/L), adsorbent dose (0.4 mg/L), contact time (160 min), temperature (300 K) and stirring speed 150 rpm. CV dye molecules ionized in water to form cations that competed with protons (H^+) of the aqueous solution at low pH value for available anionic functional groups on CLs/CLB surface. As pH value increased from 1 – 9, protonation of the aqueous solution relaxed and percentage CV dye adsorbed increased (Figure 2a). Equally, CV dye-uptake increased as the pH value of dye solution increased from 1 – 9 (Fig. S3a). The increase in percentage CV dye adsorbed and CV dye-uptake as pH value
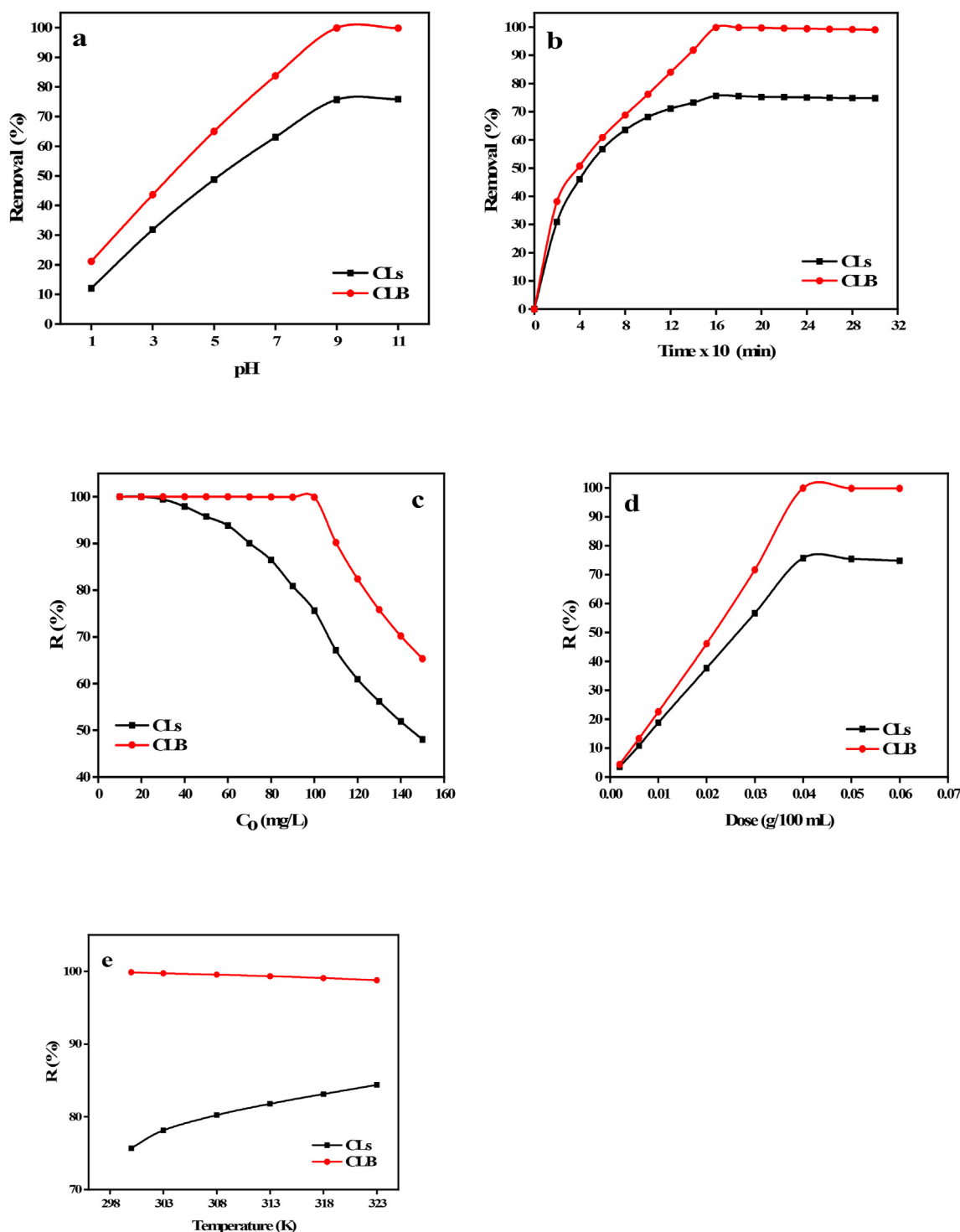
Figure 2. The effect of (a) pH, (b) contact time, (c) initial CV dye concentration, (d) adsorbent dosage and (e) temperature on adsorption of CV dye from aqueous solution.

increased from 1 – 9 might be associated with increase in electrostatic attraction between cationic dye and anionic surface charged of CLs/CLB adsorbent [38]. The maximum removal of CV dye and CV dye-uptake showing 75.82% and 189.55 mg/g for CLs and 99.87% and 249.68 mg/g for CLB confirmed CLB as a better adsorbent for removal of CV dye from aqueous solution. The insignificant difference in percentage CV dye removed and CV dye-uptake from pH 9–11 suggested pH 9 as optimum pH value for adsorption of CV dye from aqueous solution. This suggestion is in line with findings made by [39] in adsorption of toxic crystal violet

dye from aqueous solution by using waste sugarcane leaf-based activated carbon: isotherm, kinetic and thermodynamic study.

3.2.2. Effect of contact time

Contact time is part of important parameters for predicting the economy of adsorption of CV dye onto CLs and CLB adsorbents. For this reason, the effect of contact time was investigated using CLs and CLB as adsorbents at pH 9, CV dye initial concentration of 100 mg L^{-1}, adsorbent dose of 0.4 g/L, the temperature of 300 K, stirring speed of 150 rpm

and varying the contact time between 20 and 300 min. It can be seen from Figure 2b and Fig. S3b that the percentage CV dye adsorbed and CV dye-uptake increased rapidly in the first 100 min, followed by a gradual increase until 160 min of the adsorption process. The reason why the adsorption efficiency increased rapidly at first, then gradually increase and finally remains constant over time was due to the fact that the available active sites on the adsorbent surface were filled with CV dye molecules over time. This observation agreed with previous studies on the adsorption of CV dye from aqueous solution [40, 41].

3.2.3. Effect of initial CV dye concentration

The initial concentration of the adsorbate is a significant parameter in the adsorption process. To study the effect of the initial CV dye concentration on the equilibrium dye-uptake and percentage dye removal, the adsorbate concentration was varied from 10 – 150 mg/L at temperature of 300 K, pH of 9, adsorbent dose of 0.4 g/L and the mixture was stirred with the speed of 150 rpm for 160 min. A slight reduction in percentage CV dye removed from aqueous solution was noticed from the initial dye concentration of 30–100 and 50–100 mg/L in CLs and CLB respectively (Figure 2c). This might be as a result of reduction in available vacant sites for CV dye adsorption from initial CV dye concentration beyond 20 and 40 mg/L on CLs and CLB respectively. This observation predicted the existence of more available vacant sites for adsorption on CLB than CLs. The slight reduction in percentage CV dye removed from aqueous solution was followed by a noticeable decrease in percentage CV dye removal up to the initial CV dye concentration of 150 mg/L. This affirmed 100 mg/L initial dye concentration as optimum concentration for removal of CV dye from aqueous solution. Rani et al. [42] observed a similar trend in their study on the adsorption of CV dye from aqueous solution. Contrarily, CV dye-uptake increased as initial CV dye concentration increased from 10 – 150 mg/L in CLs and CLB (Fig. S3c). This might be a result of the ability of CV dye molecules to diffuse onto the surface of the adsorbent faster as initial CV dye concentration increased. A similar observation was made by [37] in the adsorption of toxic CV dye from aqueous solution.

3.2.4. Effect of adsorbent dose on CV dye adsorption

Experimental conditions to study the effect of adsorbent dose on CV dye removal are the variation of CLs and CLB dose from 0.02 – 0.60 g/L at a fixed initial CV dye concentration of 100 mg/L, contact time of 160 min, adsorption temperature of 300 K, stirring speed of 150 rpm and solution pH of 9. Experimental results show that as the dosage of CLs and CLB adsorbents increased from 0.02 – 0.40 g/L, the CV dye-uptake increased (Fig. S3d) and percentage CV dye removed from aqueous solution gradually increased from 3.52 – 75.67% and 4.36–99.87% in CLs and CLB respectively (Figure 2d). The optimal adsorbent dose for removal of CV dye was 0.40 g L^{-1} as the CV dye-uptake and percentage CV dye removed decreased as adsorbent dose increased beyond 0.4 g L^{-1}. The increase in CV dye-uptake and percentage CV dye removal could be linked to a continuous increase in the number of available active sites required for CV dye adsorption onto CLs and CLB as adsorption dose increased from 0.02 – 0.4 g/L. Beyond the adsorbent dose of 0.40 g/L, decrease in the CV dye-uptake and percentage removal observed might be due to reduction in the diffusion rate of CV dye molecules as a result of the agglomeration of adsorbent matrices as the dose increased from 0.4 – 0.6 g/L according to a previous study [5].

3.2.5. Effect of temperature

The effect of heat on the adsorption efficiency of the CLs and CLB was investigated by varying adsorption temperature between 300 and 323 K at 5 K intervals, while keeping other adsorption parameters constant. The results showed the increase in percentage CV dye adsorbed onto the CLs from 75.67% to 84.38%, while it reduced slightly from 99.87% to 98.77% for CLB as the adsorption temperature increased from 300 – 323 K (Figure 2e). A similar observation was made for CV dye-uptake using CLs and CLB as adsorbents (Fig. S3e). The increase in adsorption

efficiency of CLs as temperature increased attested to the endothermic nature of the adsorption process. It equally predicted an increase in kinetic energy and rate of collision of CV dye molecule toward CLs surface as temperature increased. On the contrary, a slight decrease in adsorption efficiency of CLB as temperature increased indicated the exothermic nature of the adsorption process, breaking of mechanical adhesion and binding forces between adsorbed CV dye molecules and CLB. These observations agreed with Khan et al. [8] in adsorption of crystal violet dye using *Platanus orientalis* (Chinar tree) leaf powder and its biochar: equilibrium, kinetics and thermodynamics study.

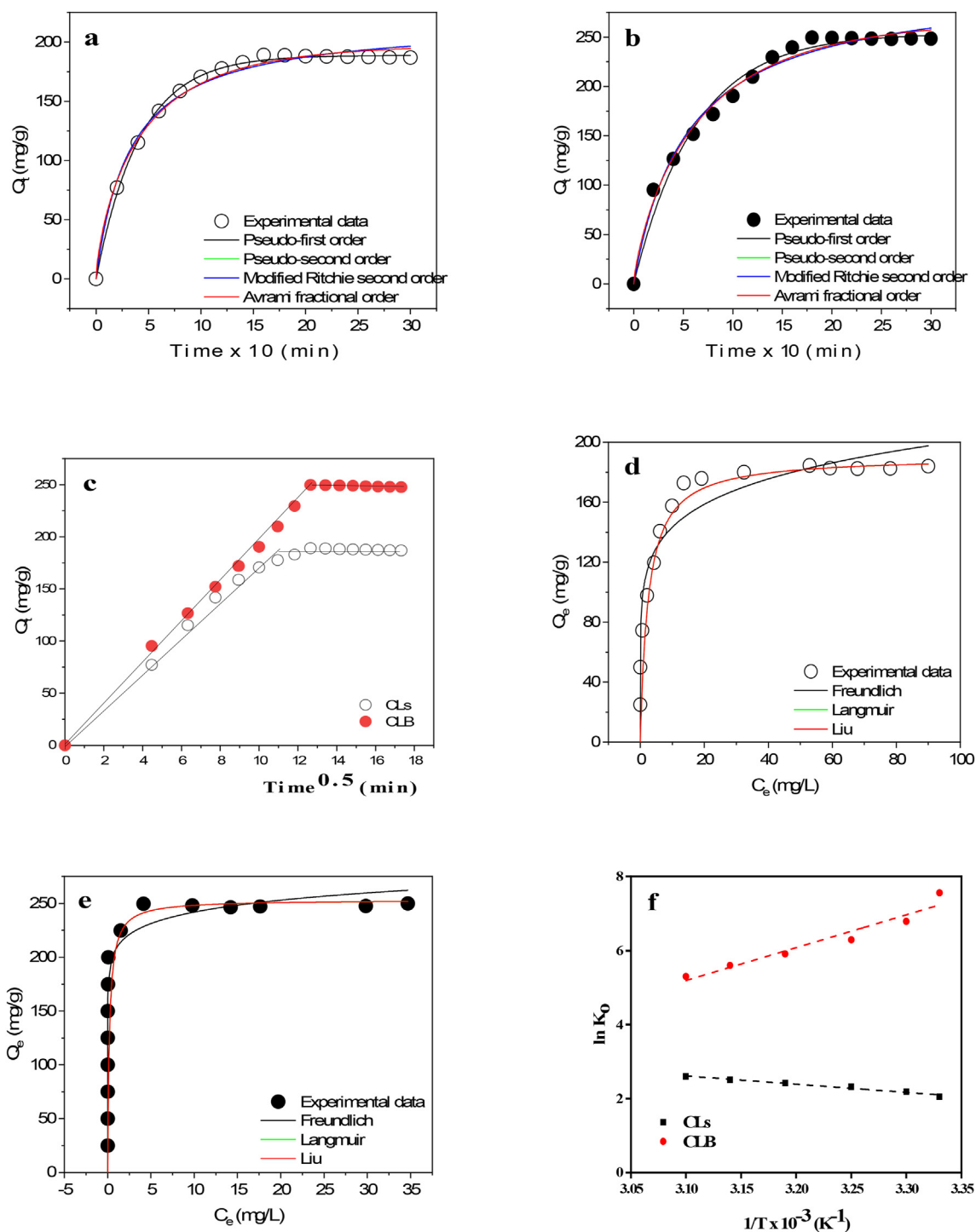## 3.3. Adsorption modeling

3.3.1. Kinetic modeling

Figure 3a and b present the kinetic curves of the CV dye adsorption onto CLs and CLB respectively, while the kinetic parameters are summarized in Table 4. Going by data in the table, the modified Ritchie second order model was the best fit of the kinetic data because this model gave the highest R^2_{adj} values (unity) and lowest SD values. As stated earlier, the closeness of experimental q ($Q_{e(expt)}$) and calculated/theoretical q ($Q_{e(calc)}$) values may not be sufficient for judging the fitness of the experimental data to kinetic models [43]. Although, the values of the $Q_{e(expt)}$ and $Q_{e(calc)}$ of the pseudo-first order model are closer, compared to other models, however, the model presented R^2_{adj} and SD values that are unfavorable. It was observed that the fitting lines of modified Ritchie second order and pseudo-second order models overlap and the two models also presented the same $Q_{e(calc)}$, but the value of pseudo-second order rate constant is zero for CLs and that the values of R^2_{adj} and SD of modified Ritchie second order model are more favorable than those of pseudo-second order model. It is therefore pertinent to discuss the modified Richie model and its parameters shown in Table 4.

A model for kinetic adsorption of gases onto porous solids was developed by Ritchie [29] and the model was modified by Cheung and co-authors [44]. Modified Ritchie kinetic equation reverts to Ritchie kinetic equation when the value of β (Ritchie's constant) is unity, which is the scenario experienced in this study. It means that there was no pre-adsorbed stage (initial loading) of CV dye onto CLs and CLB [44]. It is noted that second order rate constants for adsorption of CV dye onto CLs (0.31 min^{-1}) is lower than that of CLB (0.19 min^{-1}), that was the reason why the adsorption by CLB reached equilibrium earlier than the CLs. The higher the value of the rate constant, the faster the adsorption process. Moreover, CLB adsorbed CV dye better than CLs with adsorption capacities of 217.9 and 305.8 mg/g for CLs and CLB, respectively at the equilibrium.

The mechanism of adsorption of CV dye onto CLs and CLB was probed further by subjecting the kinetic data to the intraparticle diffusion model. The respective intraparticle curves for CLs and CLB are represented in Figure 3c and d respectively. As shown in the figures, there was 2-step mechanism for the uptake of CV dye by the two adsorbents because the intraparticle plots exhibited two linear sections [6, 45]. The first linear part was a fast adsorption process in which CV dye molecules migrated to the surface of CLs and CLB while the second linear part, which was attained after equilibrium, represented diffusion of CV dye molecules through tiny pores of CLs and CLB [32, 46].

3.3.2. Equilibrium modeling

A good choice of appropriate equilibrium model will generate equilibrium parameters that are needed for understanding adsorption mechanisms, the affinities of the adsorbents for the adsorbates as well as the surface properties. The equilibrium curves of the removal of CV dye by CLs and CLB are presented in Figure 3d and e, while the equilibrium parameters are presented in Table 5. Perusing through the table, it is evident that the best equilibrium model that describes CV dye removal is Liu. Liu model gave the lowest SD values and highest values (unity) R^2_{adj}. Liu model combines some of the features of Freundlich and Langmuir

Figure 3. Kinetic modeling of CLs (a), CLB (b), intraparticle diffusion plots (c), equilibrium modeling of CLs (d), CLB (e) and van't Hoff plot (f) of adsorption of CV dye onto CLs and CLB.

models. This model predicts that the active sites on the surface of the adsorbent will not possess equivalent energy, hence, adsorbate molecules will take preferred active sites on the surface of the adsorbent [47]. The Q_{max} values obtained for CLs and CLB for CV dye, as predicted by Liu model, are 190.7 and 253.3 mg/g, respectively. These values signified CLs and CLB as promising adsorbent materials for the removal of CV dye from aqueous solutions. CLB performed better than CLs in the removal of

CV dye molecules from solution, and this observation could be linked to the high surface area mesoporous structural nature of CLB (Table 3).

Table 6 presents the adsorption capacity (Q_{max}) values of some studies on the removal of CV dye from aqueous solutions using different bio-sorbents and biochars. Although the experiments were conducted at varying conditions, however, these data are still useful for comparison purposes. Among eight other adsorbents listed in Table 6, CLs and CLB

Table 4. Kinetic parameters of adsorption of CV dye onto CLs and CLB.

Models	Parameters	CLs	CLB
	$Q_{e(expt)}$ (mg/g)	187.9	248.7
Pseudo-first order	$Q_{e(calc)}$ (mg/g)	188.8	253.8
	k_f (1/min)	0.2400	0.1600
	R^2_{adj}	0.9981	0.9830
	SD (mg/g)	2.309	9.447
Pseudo-second order	$Q_{e(calc)}$ (mg/g)	217.9	305.8
	k_s (g/mg min)	0.0000	6.060×10^{-5}
	R^2_{adj}	0.9795	0.9848
	SD (mg/g)	5.603	8.923
Modified Ritchie second order	$Q_{e(calc)}$ (mg/g)	217.9	305.8
	k_R (1/min)	0.0310	0.0190
	β	1.000	1.000
	R^2_{adj}	1.000	1.000
	SD (mg/g)	2.007×10^{-14}	2.386×10^{-14}
Avrami fractional order	$Q_{e(calc)}$ (mg/g)	198.0	268.1
	k_{AV} (1/min)	0.0220	0.0150
	n_{Av}	0.7400	0.7900
	R^2_{adj}	0.9987	0.9993
	SD (mg/g)	1.423	1.552
Intraparticle diffusion	$k_{ipd,1}$ (mg/g min$^{0.5}$);	49.53	58.69
	C (mg/g)	13.72	9.029
	R^2_{adj}	0.9697	0.9951

Table 5. Equilibrium parameters for adsorption of CV dye onto CLs and CLB.

Models	Parameters	CLs	CLB
Freundlich	K_F (L/mg)	102.34	208.4
	$n_F \, (mg/g)(mg/L)^{-\frac{1}{n_F}}$	6.840	15.44
	R^2_{adj}	0.8593	0.7506
	SD (mg/g)	20.41	40.50
Langmuir	K_L	0.4000	4.820
	Q_{max} (mg/g)	190.7	253.3
	R^2_{adj}	0.8010	0.5004
	SD (mg/g)	9.867	11.69
Liu	K_g (L/mg)	0.4000	4.820
	Q_{max} (mg/g)	190.7	253.3
	n_g	1.000	1.000
	R^2_{adj}	1.000	1.000
	SD (mg/g)	1.562×10^{-14}	2.391×10^{-14}

Table 6. Adsorption capacities of different adsorbents for CV dye.

Adsorbent	Q_{max} (mg/g)	Q_{max} predicting model	References
Alg/Pec nanocomposite	619.22	Langmuir	[48]
Avocado seed powder	95.93	Liu	[49]
Gliricidia sepium biochar (GBC700)	125.5	Hill	[50]
Zeolite- montmorillonite	150.52	Freundlich	[51]
Almond shell	12.20	Langmuir	[52]
Rosewater extract	168.61	Freundlich	[53]
Eucalyptus camdulensis Biochar	54.70	Langmuir	[54]
Polyacrylamide-grafted *Actinidia deliciosa* peels powder (PGADP)	75.19	Langmuir	[55]
CLs	190.7	Liu	*This Study*
CLB	253.3	Liu	*This study*

absolute temperature (K) and the universal gas constant (R = 8.314 J/mol K) respectively.

The values of ΔSo and ΔHo were derived from van't Hoff plot of lnK_o Vs $\frac{1}{T}$ (Figure 3f) using Eq. (10) and tabulated in Table 7.

$$lnK_o = \frac{\Delta S^o}{R} - \frac{\Delta H^o}{RT} \tag{10}$$

The basic criterion of spontaneity is based on magnitude of the Gibbs free energy (ΔG^o kJ mol^{-1}) of the adsorption process. When the values in Table 7 were examined, it was seen that CLs and CLB adsorbents exhibited opposite thermodynamic behavior. Although, the negative values of Gibbs' free energy decoded the spontaneity of adsorption of CV dye onto both CLs and CLB. Proportional decrease in ΔG^o with the continuous increase in temperature indicated the requirement of low internal energy by CV dye to be adsorbed onto CLs as temperature increased. The situation was the opposite for the CLB adsorbent (Table 7). The negative enthalpy value signified that the adsorption process was exothermic as seen in CLB, whereas the positive value of the enthalpy signified that the adsorption process was endothermic in the adsorption of CV dye onto CLs as stated earlier. The positive value of entropy illustrated growth in randomness at CV–CLs surface boundaries as temperature increased. Whereas, a negative value of entropy displayed decrease in randomness at the CV–CLB interface as temperature increased. The results revealed that increase in temperature enhanced adsorption of CV dye onto the CLs. But for CLB, the situation is just the opposite. This observations is similar to the one made by Khan et al. [8].

3.5. Mechanism of adsorption of CV dye onto CLs/CLB

It has been stated earlier that CV dye ionized in water to form CV$^+$ and Cl$^-$ (Fig. S1). The mechanism of CV dye adsorption onto the adsorbent is a 3–steps process *viz.* film, pore and intraparticle diffusion.

The film diffusion involves migration of the CV dye molecules from aqueous solution onto the surface of the adsorbent. Unlike continuous adsorption process, film diffusion was not the rate determining step for this study (batch adsorption) according to Loulidi et al. [52]. Either pore or intraparticle diffusion or combination of the two is usually rate limiting step(s) in a typical batch adsorption system like the investigated in this study.

The pore diffusion step involves adsorption of the dye molecules onto the hollow cavities or active pore sites of the adsorbent. This adsorption process proceeds majorly *via* mechanical adhesion and/or other physical means of removing dye molecules from aqueous solution.

Intraparticle diffusion is the adsorption of the dye molecule onto the adsorbent surface through chemical or/and electrostatic attraction mechanism. Chemical mechanism involves adsorption through formation of covalent bond, van der Waals force, ionic or H–bond between N

exhibited higher Q_{max} values than six of the adsorbents, which means that CLs and CLB can favorably compete with other adsorbents for removal of CV dye from aqueous solution.

3.4. Thermodynamic study

Thermodynamic expression (Eq. 9) was used for evaluating data obtained from the effect of temperature on the adsorption of CV dye onto CLs and CLB.

$$\Delta G^o = RTlnK_o = \Delta H^o - T\Delta S^o \tag{9}$$

Where K_o is equilibrium constant, ΔG^o is Gibbs' free energy (J/mol), ΔH^o is enthalpy (J/mol), ΔS^o is entropy (J/mol K), Q_e is CV dye-uptake, C_e is CV dye concentration after the adsorption process, T and R are the

Table 7. Thermodynamic parameters for the adsorption of CV dye on CLs and CLB.

T (K)	CLs			CLB		
	ΔG^o (kJ/ mol)	ΔH^o (kJ/ mol)	ΔS^o (kJ/ mol K)	ΔG^o (kJ/ mol)	ΔH^o (kJ/ mol)	ΔS^o (kJ/ mol K)
300	-5.46	18.54	0.08	-16.79	-73.79	-0.19
303	-5.70			-16.22		
308	-6.10			-15.27		
313	-6.50			-14.32		
318	-6.90			-13.77		
323	-7.30			-12.42		

atom of CV dye molecules and –OH functional group on the surface of the adsorbent as shown in proposed reaction mechanism (Figure 4a). The electrostatic attraction mechanism depends largely on pH of the dye medium. The reason why maximum adsorptions of CV dye molecules from aqueous solution onto CLs and CLB occurred at alkaline pH 9 has been thoroughly explained in sub-section 3.2.1. At that pH of 9, anionically surface charged CLs and CLB acquired the strongest electrostatic attraction towards positively charged CV dye (Figure 4b).

Figure 3a and b show two separate regions. The first linear region was a fast adsorption process associated with pore diffusion mechanism while the second linear region, which deviated from the origin was attributed to intraparticle diffusion. The deviation of the second region from the origin indicated that rate of mass transfer of CV dye molecules onto the surface of the adsorbents is much delayed. This might be the reason why optimum removal of CV dye from aqueous solution occurred at long contact time of 160 min. Therefore, intraparticle diffusion is the sole rate controlling step in the adsorption of CV dye molecules onto CLs and CLB according to Ahmed [40].

3.6. Regeneration of CLs and CLB

Ten cycles of sorption studies were carried out to investigate reusability/regeneration of CLs and CLB as adsorbents for adsorption of CV dye from aqueous solution using NaOH (0.1 M) as eluting solvent. Sustainability of the prepared adsorbents was ascertained up to the fifth adsorption-desorption process due to removal of >70% and >50% of CV dye from aqueous solution by CLB and CLs respectively. Beyond fifth sorption process, regeneration of the adsorbents declined as < 10% of the CV dye was removed from aqueous solution by the adsorbents at the tenth regeneration cycle (Figure 5). The inability of the prepared
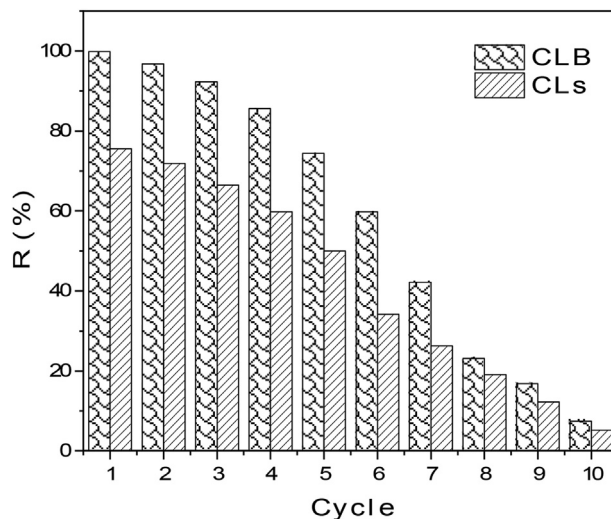
Figure 5. Regeneration of CLs and CLB as adsorbents for CV dye removal.
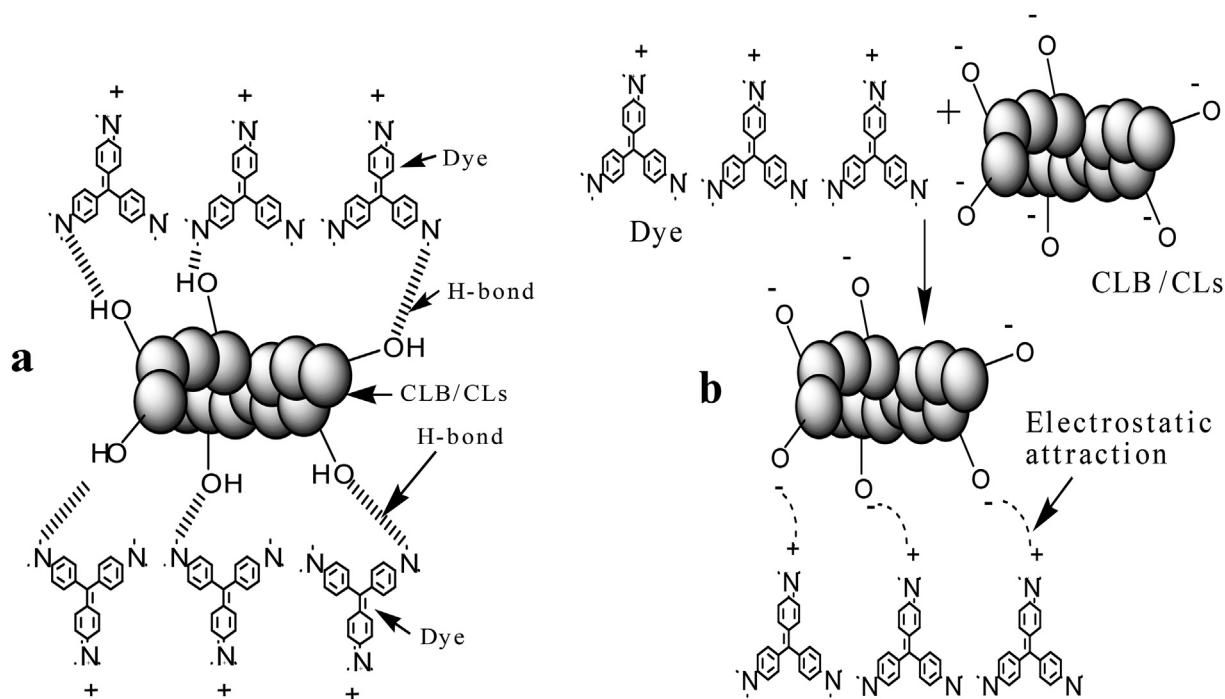
Figure 4. Proposed (a) H–bonds and (b) electrostatic attraction between CV dye and CLB/CLs.

adsorbents to remain potent beyond fifth reusability test indicated that other factors apart from electrostatic attraction were responsible for adhesion of CV dye onto CLs and CLB. Therefore, the use of only NaOH (0.1 M) as eluting solvent for regenerating the used adsorbents might not be sufficient to ascertain complete sustainability of the prepared adsorbents.

4. Conclusions

CLB was successfully synthesized from CLs through $ZnCl_2$ activation and pyrolysis. The presence of anionic –OH, –NH and –C=O as functional groups on the surface of CLs and CLB account for their ability to chemically remove cationic CV dye from aqueous solution. The high mesoporous morphological structure of CLB accounted for better mechanical removal of CV dye from aqueous solution. Removal of greater than 75 and 99% CV dye molecules from aqueous solution within 160 min presented CLs and CLB respectively as potential eco-friendly and sustainable adsorbents for removal of heavy metals and large molecular weight organic compounds from aqueous solution. The adsorption process most fitted with modified Ritchie second order kinetic and Liu isotherm model. The removal of CV dye from aqueous solution was spontaneous with CLs showing adsorption to proceed towards endothermic process, while it proceeded towards the exothermic process in CLB.

Declarations

Author contribution statement

Jamiu Mosebolatan Jabar: Conceived and designed the experiments; Contributed reagents, materials, analysis tools or data.

Matthew Ayorinde Adebayo: Contributed reagents, materials, analysis tools or data; Analyzed and interpreted the data; Wrote the paper.

Ignatius Adekunle Owokotomo: Contributed reagents, materials, analysis tools or data.

Yisau Adelaja Odusote: Contributed reagents, materials, analysis tools or data; Analyzed and interpreted the data.

Murat Yılmaz: Analyzed and interpreted the data; Wrote the paper.

Funding statement

This research did not receive any specific grant from funding agencies in the public, commercial, or not-for-profit sectors.

Data availability statement

Data will be made available on request.

Declaration of interest's statement

The authors declare no conflict of interest.

Additional information

Supplementary content related to this article has been published online at https://doi.org/10.1016/j.heliyon.2022.e10873.

References

[1] J.M. Jabar, Y.A. Odusote, Removal of cibacron blue 3G-A (CB) dye from aqueous solution using chemo-physically activated biochar from oil palm empty fruit bunch fiber, Arab. J. Chem. 13 (5) (2020) 5417–5429.
[2] Z.N. Garba, A.K. Abdullahi, A. Haruna, S.A. Gana, Risk assessment and the adsorptive removal of some pesticides from synthetic wastewater: a review, Beni-Suef Univ. J. Basic Appl. Sciences 10 (2021) 19.
[3] A. Hashem, C.O. Aniagor, G.M. Taha, M. Fikry, Utilization of low-cost sugarcane waste for the adsorption of aqueous Pb(II): kinetics and isotherm studies, Curr. Res. Green Sustain. Chem. 4 (2021), 100056.
[4] F. Pirvu, C.I. Covaliu-Mieria, I. Paun, G. Paraschiv, V. Iancu, Treatment of wastewater containing nonsteroidal anti-inflammatory drug using activated carbon materials, Materials 15 (2022) 599.
[5] J.M. Jabar, I.A. Owokotomo, Y.T. Ayinde, A.M. Alafabusuyi, G.O. Olagunju, V.O. Mobolaji, Characterization of prepared eco-friendly biochar from almond (Terminalia catappa L) leaf for sequestration of bromophenol blue (BPB) from aqueous solution, Carbon Letters (2021) 1–14.
[6] J.M. Jabar, Y.A. Odusote, K.A. Alabi, I.B. Ahmed, Kinetics and mechanisms of Congo-red dye removal from aqueous solution using activated *Moringa oleifera* seed coat as adsorbent, Appl. Water Sci. 10 (2020) 136.
[7] J.M. Jabar, Y.A. Odusote, Utilization of prepared activated biochar from water lily (Nymphaea lotus) stem for adsorption of malachite green dye from aqueous solution, Biomass Conv. Biorefinery (2021) 1–12.
[8] F.A. Khan, A. Ahad, S.S. Shah, M. Farooqi, Adsorption of crystal violet dye using *Platanus orientalis* (Chinar tree) leaf powder and its biochar: equilibrium, kinetics and thermodynamics study, Int. J. Environ. Anal. Chem. (2021) 1–21.
[9] J. Mittal, R. Ahmad, M.O. Ejaz, A. Mariyam, A. Mittal, A novel eco-friendly bionanocomposite (Alg-Cst/Kal) for the removal of crystal violet dye from its aqueous solutions, Int. J. Phytoremediation 24 (1) (2021) 1–12.
[10] A. Ahmed, K. Ansari, Enhanced sequestration of methylene blue and crystal violet dye onto pectin modified hybrid Azadirachta indica leaves powder with kaolin clay (Pect-AILP/Kal) nanocomposite, Process Biochem. 111 (2021) 132–143.
[11] S. Karthikeyan, V.K. Gupta, R. Boopathy, A. Titus, G. Sekaran, A new approach for the degradation of high concentration of aromatic amine by heterocatalytic Fenton oxidation: kinetic and spectroscopic studies, J. Mol. Liq. 173 (2012) 153–163.
[12] N.C. Dias, J.P. Bassin, G.L. Sant'Anna Jr., M. Dezotti, Ozonation of the dye reactive red 239 and biodegradation of ozonation products in a moving-bed biofilm reactor: revealing reaction products and degradation pathways, Int. Biodeterior. Biodegrad. 144 (2019), 104742.
[13] C. Felix, A. Yaroshchuk, S. Pasupathi, B.G. Pollet, M.P. Bondarenko, V.I. Kovalchuk, E.K. Zholkovskiy, Electrophoresis and stability of nano-colloids: history, theory and experimental examples, Adv. Colloid Interface Sci. 211 (2014) 77–92.
[14] A.O. Adetuyi, A.A. Mojibola, J.M. Jabar, Thermo-kinetics studies of dye removal with kaolin from Tectona grandis and indigo dye effluents, Pak. J. Sci. Indus. Res, A: Phys. Sci. 56 (2) (2013) 93–99.
[15] P.S. David, A. Karunanithi, N.N. Fathima, Improved filtration for dye removal using keratin-polyamide blend nanofibrous membranes, Environ. Sci. Pollut. Control Ser. 27 (2020) 45629–45638.
[16] A. Rafiq, M. Ikram, S. Ali, F. Niaz, M. Khan, Q. Khan, M. Maqbool, Photocatalytic degradation of dyes using semiconductor photocalysts to clean industrial water pollution, J. Ind. Eng. Chem. 97 (25) (2021) 111–128.
[17] V.K. Gupta, A. Nayak, S. Agarwal, Bioadsorbents for remediation of heavy metals: current status and their future prospects, Environ. Eng. Res. 20 (1) (2015) 1–18.
[18] Y.W. Kim, J. Kim, D.H. Moon, H. Shin, Adsorption and precipitation of anionic dye Reactive Red 120 from aqueous solution by aminopropyl functionalized magnesium phyllosilicate, Kor. J. Chem. Eng. 36 (1) (2018) 101–108.
[19] A.O. Adetuyi, J.M. Jabar, O.O. Obaseki, A.V. Popoola, Adsorption of C.I. vat blue I (indigo) from simulated dyeing effluent on some prepared activated bio-solids, Asian dyers 6 (3) (2009) 42–47.
[20] A.O. Adetuyi, J.M. Jabar, Adsorption isotherm studies of indigo on some activated agro-solid wastes, Asian dyers 7 (3) (2010) 46–49.
[21] A.O. Adetuyi, J.M. Jabar, Kinetic and thermodynamic studies of indigo adsorption on some activated bio-solids, J. Chem. Soc. Pakistan 33 (2) (2011) 158–165.
[22] J.M. Jabar, Pyrolysis: a convenient route for production of eco-friendly fuels and precursors for chemical and allied industries, IntechOpen 1–15 (2021).
[23] P.S. Thue, D.R. Lima, M. Naushad, E.C. Lima, Y.R.T. de Albuquerque, S.L.P. Dias, M.R. Cunha, G.L. Dotto, I.A.S. de Brum, High removal of emerging contaminants from wastewater by activated carbons derived from the shell of cashew of Para, Carbon Letters 31 (1) (2020) 1–16.
[24] X. Liu, X. Zhang, Z. Li, R. Feng, Y. Zhang, Characterization of corncob-derived biochar and pyrolysis kinetics in comparison with corn stalk and sawdust, Bioresour. Technol. 170 (2014) 76–82.
[25] M.F. Adesemuyi, M.A. Adebayo, A.O. Akinola, E.F. Olasehinde, K.A. Adewole, L. Lajide, Preparation and characterisation of biochars from elephant grass and their utilisation for aqueous nitrate removal: effect of pyrolysis temperature, J. Environ. Chem. Eng. 8 (2020), 104507.
[26] O.A.A. Eletta, F.O. Ayandele, J.O. Ighalo, Adsorption of Pb(II) and Fe(II) by mesoporous composite activated carbon from *Tithonia diversifolia* stalk and *Theobroma cacao* pod, Biomass Conv. Biorefinery (2021) 1–10.
[27] G.A. Idowu, A.F. Aiyesanmi, F.O. Oyegoke, Organochlorine pesticide residues in pods and beans of cocoa (Theobroma cacao L) from Ondo State Central District, Nigeria, Environ. Adv. 7 (2022), 100162.
[28] L. Armengot, M.J. Beltran, M. Schneider, X. Simon, D. Perez-Neira, Food-energy-water nexus of different cacao production systems from a LCA approach, J. Clean. Prod. 304 (2021), 126941.
[29] A.G. Ritchie, Alternative to Elovich equation for kinetics of adsorption of gases on solids, J. Chem. Soc., Faraday Trans. 73 (1977) 1650–1653.
[30] Y. Liu, H. Xu, S.F. Yang, J.H. Tay, A general model for biosorption of Cd^{2+}, Cu^{2+} and Zn^{2+} by aerobic granules, J. Biotechnol. 102 (2003) 233–239.
[31] M.A. Adebayo, F.I. Areo, Removal of phenol and 4-nitrophenol from wastewater using a composite prepared from clay and *Cocos nucifera* shell: kinetic, equilibrium and thermodynamic studies, Res. Environ. Sustain. 3 (2021), 100020.
[32] T.J. Popoola, A.E. Okoronkwo, O.O. Oluwasina, M.A. Adebayo, Preparation, characterization, and application of a homemade graphene for the removal of Congo red from aqueous solutions, Environ. Sci. Pollut. Res. 28 (37) (2021) 52174–52187.

[33] O.S. dos Santos Escobar, C.F. de Azevedo, A. Swarowsky, M.A. Adebayo, M.S. Netto, F.M. Machado, Utilization of different parts of Moringa Oleifera Lam. seeds as biosorbents to remove Acid Blue 9 synthetic dye, J. Environ. Chem. Eng. 9 (4) (2021), 105553.

[34] A.H. Jawad, R.A. Rashid, K. Islam, S. Sabar, High surface area mesoporous activated carbon developed from coconut leaf by chemical activation with H_3PO_4 for adsorption of methylene blue, Desalination Water Treat. 74 (2017) 326–335.

[35] G.A. Idowu, A.J. Fletcher, The manufacture and characterisation of rosid angiosperm-derived biochars applied to water treatment, BioEnergy Res. 13 (2019) 387–396.

[36] A.H. Jawad, M. Bardhan, MdA. Islam, MdA. Islam, S.S.A. Syed-Hassan, S.N. Surip, Insight into the modeling, characterization and adsorption performance of mesoporous activated carbon from corn cob residue *via* microwave- assisted H_3PO_4 activation, Surface. Interfac. 21 (2020), 100688.

[37] R. Kumar, R. Ahmad, Biosorption of hazardous crystal violet dye from aqueous solution onto treated ginger waste (TGW), Desalination 265 (2011) 112–118.

[38] R. Nithya, A. Thirunavukkarasu, C. Sivasankari, Comparative Profile of green and Chemically Synthesized Nanomaterials from Bio-Hydrometallurgical Leachate of E-Waste on crystal Violet Adsorption Kinetics, Thermodynamics, and Mass Transfer and Statistical Models, Biomass Conversion and Biorefinery, 2022, p. 2022.

[39] S.A. Patil, P.D. Kumbhar, B.S. Satvekar, N.S. Harale, S.C. Bhise, S.K. Patil, A.S. Sartape, S.S. Kolekar, M.A. Anuse, Adsorption of toxic crystal violet dye from aqueous solution by using waste sugarcane leaf-based activated carbon: isotherm, kinetic and thermodynamic study, J. Iran. Chem. Soc. 19 (2022) 2891–2906.

[40] R. Ahmad, Studies on adsorption of crystal violet dye from aqueous solution onto coniferous pinus bark, J. Hazard Mater. 15 (2009) 767–773.

[41] J.M. Jabar, Y.A. Odusote, Y.T. Ayinde, M. Yılmaz, African almond (*Terminalia catappa* L) leaves biochar prepared through pyrolysis using H_3PO_4 as chemical activator for sequestration of methylene blue dye, Results Eng. 14 (2022) 100385.

[42] S. Rani, S. Chaudhary, Adsorption of methylene blue and crystal violet dye from waste water using Citrus limetta peel as an adsorbent, Mater. Today Proc. 60 (2022) 336–344.

[43] M.A. Adebayo, J.I. Adebomi, T.O. Abe, F.I. Areo, Removal of aqueous Congo red and Malachite green using Ackee apple seed–bentonite composite, Colloid Interf Sci. Commun. 38 (2020), 100311.

[44] C.W. Cheung, J.F. Porter, G. McKay, Sorption kinetic analysis for the removal of cadmium ions from effluents using bone char, Water Resour. 35 (2001) 605–612.

[45] M.A. Adebayo, L.D.T. Prola, E.C. Lima, M.J. Puchana-Rosero, R. Cataluña, C. Saucier, C.S. Umpierres, J.C.P. Vaghetti, L.G. da Silva, R. Ruggiero, Adsorption of Procion Blue MX-R dye from aqueous solutions by lignin chemically modified with aluminium and manganese, J. Hazard Mater. 268 (2014) 43–50.

[46] M.C. Ribas, M. Franco, M.A. Adebayo, G.M. Parkes, E.C. Lima, L.A. Féris, Adsorption of procion red MX-5B dye from aqueous solution using a homemade peach activated carbon compared with commercial activated carbon, Appl. Water Sci. 10 (6) (2020) 154.

[47] F.M. Machado, C.P. Bergmann, E.C. Lima, M.A. Adebayo, S.B. Fagan, Adsorption of a textile dye from aqueous solutions by carbon nanotubes, Mater. Res. 17 (Suppl. 1) (2014) 153–160.

[48] A. Mirza, R. Ahmad, An efficient sequestration of toxic crystal violet dye from aqueous solution by Alginate/Pectin nanocomposite: a novel and ecofriendly adsorbent, Ground Water Sustain. Dev. 11 (2020), 100373.

[49] A. Bazzo, M.A. Adebayo, S.L.P. Dias, E.C. Lima, J.C.P. Vaghetti, E.R. de Oliveira, A.J.B. Leite, F.A. Pavan, Avocado seed powder: characterization and its application as biosorbent for crystal violet dye removal from aqueous solutions, Desalination Water Treat. 57 (34) (2016) 15873–15888.

[50] A. Wathukarage, I. Herath, M.C.M. Iqbal, M. Vithanage, Mechanistic understanding of crystal violet dye sorption by woody biochar: implications for wastewater treatment, Environ. Geochem. Health 41 (2017) 1647–1661.

[51] M. Sarabadan, H. Bashiri, S.M. Mousavi, Removal of crystal violet dye by efficient and low cost adsorbent: Modeling, Kinetic Equilibrium Stud. Korean J. Chem. Eng. 36 (10) (2019) 1575–1586.

[52] I. Loulidi, F. Boukhlifi, M. Ouchabi, A. Amar, M. Jabri, A. Kali, S. Chraibi, C. Hadey, F. Aziz, Adsorption of crystal violet onto an agricultural waste residue: kinetics, isotherm, thermodynamics, and mechanism of adsorption, Sci. World J. (2020), 5873521.

[53] Z. Falaki, H. Bashiri, Preparing an adsorbent from the unused solid waste of Rosewater extraction for high efficient removal of Crystal Violet, J. Iran. Chem. Soc. 18 (2021) 2689–2702.

[54] M.T. Amin, A.A. Alazba, M. Shafiq, Successful Application of *Eucalyptus camdulensis* biochar in the batch adsorption of crystal violet and methylene blue dyes from aqueous solution, Sustainability 13 (2021) 3600.

[55] R. Ahmad, K. Ansari, Polyacrylamide-Grafted *Actinidia deliciosa* peels powder (PGADP) for the sequestration of crystal violet dye: isotherms, kinetics and thermodynamic studies, Appl. Water Sci. 10 (2020) 195.